Supporting Information

Preparation of the Cyclopentazole Anion in the Bulk – A Computational Study

Uzi Geiger and Yehuda Haas*

Institute of Chemistry

The Hebrew University of Jerusalem, Jerusalem, Israel

1. Model system – calculations on methyl pentazole

   1.1. Electronic energies

   Table S1 presents the ΔE_{elec} of several processes of the MeP-RA system calculated using a variety of methods at the M06/aug-cc-pVDZ and BMC-CCSD optimized geometries (see section 1.2 for choice of geometric optimization method). These results are compared with the higher level W1BD//BMC-CCSD calculations. Changes of geometry optimization methods typically leads to a small difference (lower than 1 kcal/mol in electronic energies). $\Delta E_2^{\ddagger}$ calculation by HF appears to be the only exception.

Table S1. Calculated electronic energy differences of the MeP-RA system using several methods in the M06/aug-cc-pVDZ and BMC-CCSD optimized gepmetries. Kcal/mol. IP is the first ionization potential of the RA, equal in size to the electron affinity of the neutral; ΔE is the electron energy difference upon reaction, $\Delta E^{\ddagger}$ the reaction barrier.

	Quantity	IP		$\Delta E^{\ddagger}_1$		$\Delta E^{\ddagger}_2$		ΔE_1		ΔE_2	
	Optimization method	M06	BMC-CCSD	M06	BMC-CCSD	M06	BMC-CCSD	M06	BMC-CCSD	M06	BMC-CCSD
Electronic method	**W1BD**		**-4.6**		**11.8**		**20.1**		**-27.9**		**-6.6**
	G4(MP2)	-3.5	-3.5	11.2	11.3	21.8	21.2	-28.7	-29.4	-6.7	-6.7
	CBS-4M	0.3	0.4	13.7	13.2	24.8	26.0	-19.8	-20.3	-2.9	-2.6
	CBS-QB3	-3.8	-3.8	11.6	12.2	20.0	19.6	-25.3	-25.8	-6.0	-6.0
	G3SX	-4.1	-4.0	10.9	11.1	18.9	18.2	-28.6	-29.2	-5.8	-5.8
	G3SX(MP2)	-3.5	-3.4	10.6	10.7	18.6	17.9	-29.7	-30.4	-6.0	-6.0
	MCG3/3	-3.0	-2.9	10.0	10.4	17.1	16.0	-29.2	-29.9	-6.1	-6.1
	MCG3-MPW	-2.9	-2.9	11.2	11.3	19.7	19.3	-27.6	-28.2	-5.4	-5.4
	BCM-CCSD	-4.0	-3.9	10.5	10.7	20.9	19.9	-29.6	-30.3	-6.5	-6.4
	BMC-QCISD	-4.5	-4.5	11.4	11.4	22.9	22.0	-30.3	-30.9	-7.1	-7.0
	MC-QCISD/3	-2.8	-2.7	12.3	12.2	24.0	22.6	-30.6	-31.4	-6.2	-6.2
	MC3BB	-11.8	-11.8	12.9	12.6	28.4	29.2	-23.7	-24.0	-9.4	-9.3
	MC3MPW	-9.9	-9.8	13.1	12.9	30.1	30.6	-21.1	-21.3	-10.7	-10.6
	MC3TS	-12.7	-12.7	11.7	11.8	28.9	28.9	-25.0	-25.2	-12.9	-13.0
	M06	0.3	0.2	12.3	11.9	20.0	21.7	-19.6	-19.6	-2.3	-2.2
	B3LYP	-14.1	-14.2	11.5	11.7	17.4	19.3	-20.7	-20.8	-6.0	-6.1
	HF	-17.0	-16.6	17.3	17.7	27.3	33.4	-48.6	-49.6	-17.7	-16.7

Several methods used with the M06/aug-cc-pVDZ optimized geometries are in good agreement with the W1BD//BMC-CCSD results, most notably G3SX, MCG3-MPW, and BMC-CCSD with an RMSD of 0.87, 0.97, and 1.08 kcal/mol, respectively. It was, however, found that an even better agreement could be obtained by using the average result of a few methods. Thus, the average of G3SX, CBS-QB3, and BMC-QCISD at the M06/aug-cc-pVDZ optimized geometries (denoted Avg-C//M06/aug-cc-pVDZ) shows an RMSD of 0.42 kcal/mol from the W1BD//BMC-CCSD values and a maximum absolute deviation of 0.53 kcal/mol (Table S2). The RMSD of Avg-C//M06/aug-cc-pVDZ from W1BD//BMC-CCSD, including the ZPE, is calculated to be ~0.55 kcal/mol

Table S2. Calculated electronic energy differences (kcal/mol) of MeP-RA at the W1BD//BMC-CCSD and Avg-C//M06/aug-cc-pVDZ level of theories.

Quantity	IP	$\Delta E^{\ddagger}_1$	$\Delta E^{\ddagger}_2$	ΔE_1	ΔE_2
W1BD//BMC-CCSD	-4.6	11.8	20.1	-27.9	-6.6
Avg-C//M06/ aug-cc-pVDZ	-4.2	11.3	20.6	-28.0	-6.3
difference	0.48	-0.53	0.49	-0.18	0.29

The Avg-C//M06/aug-cc-pVDZ method, which scales as N^7 is computationally feasible for PP-RA calculations; for larger systems the cheaper BMC-CCSD//M06/aug-cc-pVDZ method (scales as N^6) will be used. BMC-CCSD//M06/aug-cc-pVDZ is calculated to have a total RMSD of ~1.2 kcal/mol from W1BD//BMC-CCSD values, including ZPE.

1.2. Geometries and frequencies

The geometries and frequencies of MeP-RA, its transition states, and products were computed using HF, 2 DFT functionals (B3LYP and M06) and 3 multi-coefficient extrapolated DFT methods (MC3BB, MC3MPW, and MC3TS) that are all applicable to larger ArP-RA systems. Table S3 presents the ΔZPE and ΔS deviations of the lower methods from the benchmark and the benchmark results. All data in table S3 are relative to MeP-RA – although the absolute values could be compared, only the relative values are of practical use and error cancelation improves accuracy.

Table S3. ΔZPE and ΔS Deviations (kcal/mol) of several calculation methods from the benchmark (BMC-CCSD), ΔZPE and ΔS values of the benchmark, and RMS deviation.

		MeP	TS1	TS2	MeA-RA + N2	Me-R + N5	RMSD
ΔΔZPE: Deviation from BMC-CCSD values	**HF/ aug-cc-pVTZ**	0.35	-0.40	-2.04	-1.26	-0.41	1.11
	B3LYP/GTbas3	0.08	-0.09	0.17	-0.02	0.36	0.19
	M06/ aug-cc-pVDZ	-0.06	-0.20	0.19	0.22	0.12	0.17
	MC3BB	-0.04	0.03	0.99	-0.11	0.00	0.45
	MC3MPW	-0.10	0.04	1.52	-0.09	-0.05	0.68
	MC3TS	-0.10	0.14	1.96	0.05	-0.08	0.88
ΔZPE	**BMC-CCSD**	2.24	-2.02	-2.11	-4.29	-4.84	
ΔΔS: Deviation from BMC-CCSD values (cal/mol*K)	**HF/ aug-cc-pVTZ**	6.37	-0.38	5.56	0.57	1.04	3.82
	B3LYP/GTbas3	-0.01	0.33	-0.33	-3.83	0.12	1.73
	M06/ aug-cc-pVDZ	0.08	0.63	0.06	1.82	2.63	1.46
	MC3BB	6.44	-0.06	0.79	0.32	0.16	2.91
	MC3MPW	6.31	-0.06	0.34	0.50	0.31	2.84
	MC3TS	5.12	-0.21	0.15	0.25	0.36	2.30
ΔS (cal/mol*K)	**BMC-CCSD**	-5.06	1.23	2.10	41.06	35.61	

The best approximation to the benchmark is achieved with the M06 functional geometries and frequencies. M06/aug-cc-pVDZ ΔZPE values deviate from BMC-CCSD ones by 10% or less. ΔZPE values should be compared to total energies differences which are ~10 and 20 kcal/mol for TS1 and TS2, respectively, using BMC-CCSD values, and to the electronic energy error that is not expected to be less than 0.5 kcal/mol. This indicated that M06/aug-cc-pVDZ ZPE can be used as substitution for higher level methods in this and similar systems.

The geometries of TS1 and TS2 at the BMC-CCSD and M06/aug-cc-pVDZ levels are shown in figure S1, values of active bond distances (Å) are highlighted. M06/aug-cc-pVDZ geometries are representative of all lower level geometries. While TS1 has similar geometries in all computational levels, the C—N bond distances are different by only ~0.1 Å. The case of TS2 is more complicated – The BMC-CCSD geometry shows distinct concerted characteristics while all lower levels are compatible with sequential bond breaking mechanism (no stable intermediate is localized , but the elongations of

the two NN bonds that eventually break to form N_2 are distinctly different). The results indicate a very "floppy" transition state. This supports the suitability of the energetic values calculated at the M06/aug-cc-pVDZ geometry (with M06/aug-cc-pVDZ ZPE) while large differences in geometric particulars are found between these and BMC-CCSD level geometries.

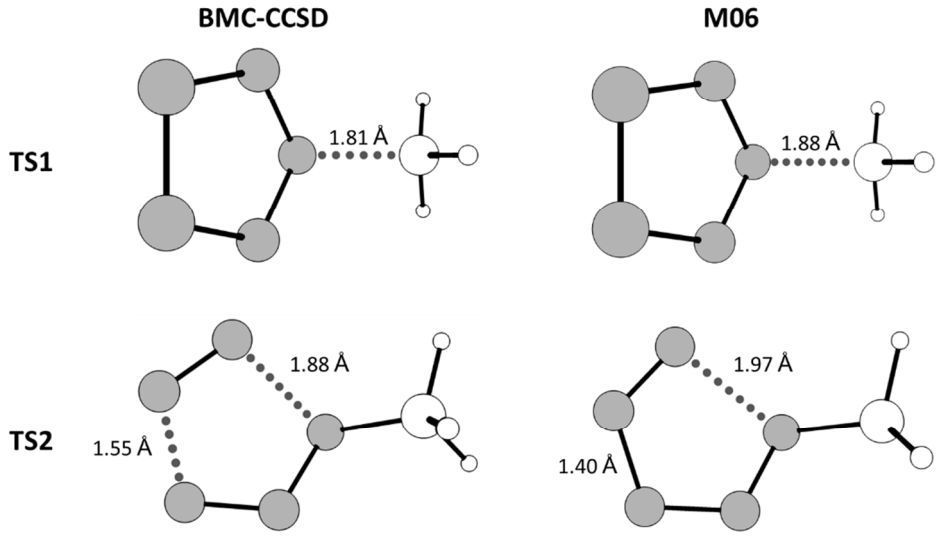

Figure S1. Geometries TS1 and TS2 of MeP-RA calculated at the M06*/aug-cc-pVDZ* and BMC-CCSD levels. Lengths of active bonds are indicated.

2. Comparison of calculated and experimental data.

As our main investigation method incorporates several assumptions (adequacy of DFT geometries for radical anions, accuracy of single point calculated energy, and neglect of entropic effects). The suitability of the calculation was validated by comparison with empirical data from the literature. The system selected for comparison was the dehalogenation reaction of halogenated aryl radical anions. These molecules have much in common with aryl pentazoles radical anions – the added electron has a π symmetry, they tend to become more planar upon addition of an electron, the C—X bond weakens in the radical anions relative to the neutral molecules, and upon reaction the electron changes symmetry to σ in the resulting aryl radical (implying PES crossing and molecular symmetry breaking in the transition state). Experimental data were collected from references 20, 42-46 and include reaction rates at room temperature of relatively small aryl chloride radical anions (larger molecules were excluded because of computational cost, bromides were

excluded because the 6-31B(d) basis set, used in both BMC-CCSD and BMC-QCISD methods, does not include parameters for the bromide atom). These data were compared with the computed reaction barriers using the BMC-CCSD//M06/aug-cc-pVDZ method (see Table S1 and Figure); a good linear relation between the two was found. Most of the deviations are attributed to differences in pre-exponential factors of the Arrhenius equation for different compounds.

Table S1: experimental log(k) and BMC-CCSD//M06/aug-cc-pVDZ barrier heights of chloro aryl radical anion dearilation reactions in DMF.

Compound	**log(k)**	**Barrier (kcal/mol)**
3-chloroacetophenone	1	17.70
2-chlorobenzaldehyde	2.3	17.67
4-chloroacetophenone	5.5	12.61
4-chloroquinoline	5.8	13.53
3-chlorobiphenyl	5.85	11.98
1-chloronaphthalene	7.2	9.49
2-chloronaphthalene	8	6.69
4-chlorobiphenyl	8.65	6.59
2-chlorobiphenyl	10.85	1.59

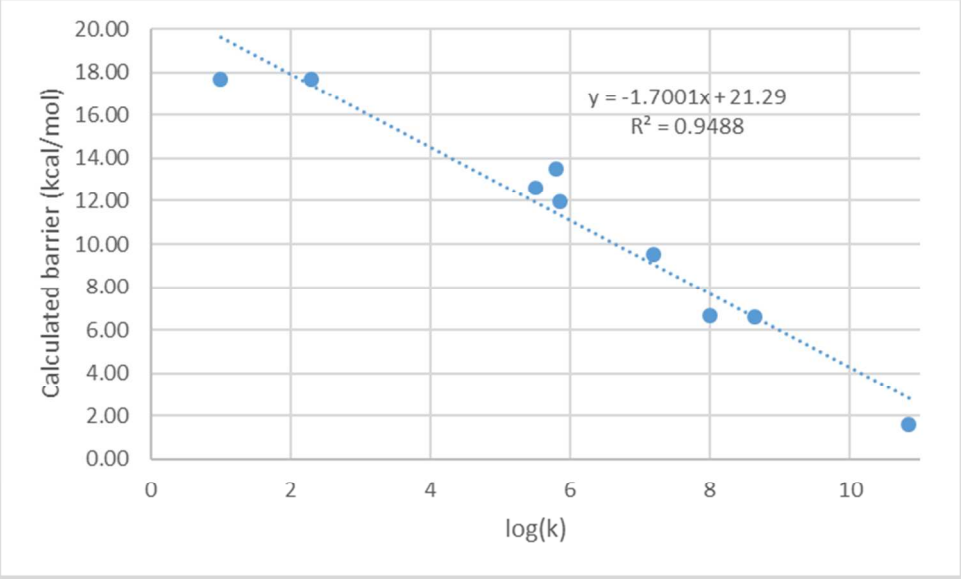

Figure S2: a graphic representation of the data in Table S1. The slope of the trend line yields a temperature of 296 K (experiments were performed at room temperature of 20-25 °C, see refs 42-47).

3. Substituted PP-RAs

The ArP- RAs studied computationally are listed in Figure S3.

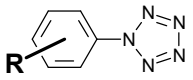

PP	(R=H)	oTFM	(R=o-CF_3)
TFMPP	(R=p-CF_3)	oMePP	(R=o-CH_3)
FPP	(R=p-F)	oFPP	(R=o-F)
MePP	(R=p-CH_3)		
MeOPP	(R=p-OCH_3)		

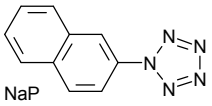

Figure S3. ArP-RAs investigated in this work and their acronyms.

Tables S5 and S6 report the results obtained for some substituted PP-RAs and of NaP-RA. While most activation energies are only slightly affected by para substitution of PP-RA, the calculated reaction enthalpy of R_1 is reduced 30% upon changing the substitution from the most EWG (trifluoromethyl) to the most EDG (methoxy). Strong EDGs are therefore favorable for the synthesis of cyclo-N_5^-, both by the aforementioned effect and the increased stability of the neutral ArP starting materials. Minor differences are revealed on comparing phenyl to naphtyl pentazol. Thus aromatic system expansion does not materially affect the character of the system. These results are consistent with the view that the aryl pentazole radical anions are π radicals while the aryl radicals are σ ones, thus negating any stabilization of the resulting aryl radical upon expansion of the aromatic system.

Table S5. Calculated IPs, reaction parameters, and total energies of para substituted ArP-RAs and NaP-RA. BMC-CCSD//M06/aug-cc-pVDZ data in kcal/mol, total energies in Hartree.

	PP-RA	**TFMPP-RA**	**FPP-RA**	**MePP-RA**	**MeOPP-RA**	**NaP-RA**
Total ArP-RA energy	-543.86731	-841.40004	-603.80252	-543.86682	-618.99999	-657.99639
IP	62.6	66.0	61.4	60.5	58.7	60.8
$\Delta E^{\ddagger}1$	26.1	28.3	25.0	25.5	24.5	25.5
$\Delta E^{\ddagger}2$	25.6	25.3	24.4	24.9	23.6	24.6
ΔE1	14.9	18.5	14.3	13.9	12.8	14.3
ΔE2	-42.5	-40.7	-38.5	-41.5	-36.1	-40.9

Table S6. Calculated change in IPs and reaction parameters of ortho substituted ArP-RAs relative to their para counterparts. BMC-CCSD//M06/aug-cc-pVDZ data in kcal/mol, total energies in Hartree.

	oFPP-RA	**oMePP-RA**	**oTFMPP-RA**
Total ArP-RA energy	-603.79693	-543.86222	-841.38885
ΔIP	0.4	-2.1	-3.3
$\Delta\Delta E^{\ddagger}1$	-3.6	-3.3	-5.8
$\Delta\Delta E^{\ddagger}2$	-2.5	-3.6	-4.0
ΔΔE1	-2.2	-3.4	-6.3
ΔΔE2	-4.8	-3.6	-3.0

Changing substitution site from para to ortho results in a reduction in all reaction parameters. The effect appears to correlate with the size – it becomes more pronounced for the more voluminous active group is, especially for $\Delta E^{\ddagger}1$.

In consequence, these calculations imply that substitution effects do not materially affect changes in the outcome of the ArP-RA's reactions.